

## Input Current THD Reduction via Virtual Resistant in EV Charger

A. Mohammadi, M.A. Shamsi Nejad\*

Department of Electrical and Computer Engineering, University of Birjand, Birjand, Iran

**Abstract-** This paper investigates a fundamental issue in AC-DC rectifiers that are specifically used as charger for electric vehicle (EV), i.e. the total harmonic distortion (THD) of input current waveforms. Firstly, the topology of two-stage charger along with the corresponding control scheme is reviewed. Then, the research gap namely high harmonic distortion of input current is identified and analyzed. A revision of the conventional control method with the aid of virtual resistant is proposed and investigated from the circuit perspectives. Finally, simulation results are delivered to validate the analysis and the reduction of THD in the input current waveform. This proposed method, the steady state is studied.

**Keyword:** Battery charger, Electric vehicle, Inverter, Rectifier, Virtual resistance

### NOMENCLATURE

D	Duty-cycle
EVs	Electric vehicles
F-bridge	Full bridge
G2V	Grid-to-Vehicle
H-bridge	Half bridge
$I_{cf}$	Filter capacitor current
$I_{in}$	Input current of rectifier
$I_{ac}$	Current of the network input
$I_s$	Source current
$i_{TB}^*$	Current reference received from the battery
$i_{in}^*$	Input reference current of the charger
PFC	Power-factor-correction
PHEVs	Plug-in hybrid electric vehicles
PWM	Pulse width modulation
PLL	Phase-locked loop
$R_{1,2,3,4}$	Virtual resistance
THD	Total harmonic distortion
V2H	Vehicle-to-Home
$V_{cf}$	Filter capacitor voltage
$V_{ac}$	Voltage of the network input
$V_{dc}$	DC-link voltage

### 1. INTRODUCTION

In recent years, there has been increasing interest in various eco-friendly vehicles such as electric vehicles (EVs) and plug-in hybrid electric vehicles (PHEVs), which have a significant potential to reduce environmental pollution [1-3]. An important part of the structure of

electric vehicles is its charger. However, chargers are divided into two categories: on-board and off-board. Each has some advantages and disadvantages stated in [2]. In the off-board type, the amount of power and efficiency is important. And in the on-board type, the size, cost, and weight are important. In addition, because the charger is installed in the EV, it must be small, lightweight, and have a long lifetime [4]. An important advantage of the on-board charger is easy access to city electricity that has increased the use of this type of car, especially in light cars. Therefore, this article examines the on-board charger. Conventional on-board chargers for EVs are based on isolated AC-DC converters with the two stages structure consisting of a power-factor-correction (PFC) stage and a DC-DC power-conversion stage [5-7]. The PFC stage, which is usually a boost converter, converts input AC voltage to DC-link voltage with a unity power factor [8], whereas the DC-DC power-conversion stage, which is usually an isolated high-frequency DC-DC converter, regulates the output power and provides galvanic isolation for user safety [9]. This structure has advantages such as accepting wide input voltage, providing a high power factor and well-regulated output power. However, the two-stage structure also has many disadvantages, such as low efficiency and circuit complexity because of its two power-processing stages. Another major drawback is a bulky intermediate DC-link capacitor that filters power fluctuations. The high current flowing through the intermediate DC-link capacitor also causes significant power loss and considerably reduces the capacitor lifetime, leading to capacitor failure [10-11]. To eliminate the PFC stage and reduce the DC-link capacitance, single-stage

Received: 11 Oct. 2020

Revised: 07 Nov. 2020

Accepted: 12 Nov. 2020

\*Corresponding author:

E-mail: [mshamsi@birjand.ac.ir](mailto:mshamsi@birjand.ac.ir) (M. Shamsi Nejad)

Digital object identifier: 10.22098/joape.2021.7869.1555

**Research Paper**

© 2021 University of Mohaghegh Ardabili. All rights reserved.

approaches are being investigated to replace two-stage structures [12-13]. In single-stage converters with a DC-link capacitor, the PFC stage and the DC-DC stage are merged by sharing the switches. However, because the DC-link voltage is not controlled in this scheme, it can be more than twice the grid voltage, leading to requirement of high voltage rating switches which causes high switching and conduction losses. In addition, because PFC is achieved based on the operation principle of the circuit without an additional PFC controller, the power factor is affected by changes in the grid voltage or load condition [14]. To achieve a high power factor without a PFC stage and a DC-link capacitor, single-stage resonance converters with inherent PFC and current-fed full-bridge converters have been introduced [15-18]. These converters do not require a DC-link capacitor, thereby eliminating the associated problems. Also almost unity power factor can be achieved using the appropriate PFC-control techniques. However, these single stage converters contain many components and an input bridge diode that not only causes high conduction losses but also requires additional heat management. To overcome these drawback, single-stage bridgeless topologies based on two-stage boost-fly back converter and half-bridge PFC converter have been investigated [19-21]. However, such converters are suitable only for low power applications because the applied topologies normally imply high electrical stresses. Due to these reasons, the isolated bridgeless type converters for high power capability ( $>1$  KW) has rarely been studied. Nowadays, two main EVs charging solutions are being investigated: the inductive and the conductive methods. In the conductive method there is an electrical contact between the vehicle and the power grid, and in the inductive method there is no electrical contact between the vehicle and the power grid [19]. Although the recent progresses in the inductive method [20-21], the most common solution are based on the conductive method [22]. The majority of EVs are being designed with conductive method on-board unidirectional battery chargers specified by IEC 61851-1 standard, mode 1, 2, and 3 [23]. These unidirectional battery chargers only permit operation in Grid-to-Vehicle (G2V) mode, in which the traction batteries are charge from the power grid. In addition to on-board battery chargers, some vehicles allow the possibility of charging their batteries with off-board unidirectional chargers, specified by IEC 61851-1 standard mode 4. Various solutions for battery chargers of EVs operating in G2V mode have been proposed in recent years. In Ref. [24], a battery charger for PHEVs based on the buck converter with

controllable power factor is proposed. This topology is composed by a single-stage H-bridge aiming to reduce the size and weight of the charger. Besides the conventional bridge boost PFC topologies [16, 25]. In Ref. [26] an overview of the bridgeless boost PFC topologies is presented. In Ref. [27] an innovative topology based on a three-phase ultra-spars matrix converter is presented, which absorbs current with low total harmonic distortion and nearly unitary power factor over a wide output power range, from zero to full load. In Ref. [28] a bidirectional battery charger for PHEVs that can operate in the G2V, V2G and Vehicle-to-Home (V2H) modes is proposed. Figure 1 presents the electric diagram of the proposed reconfigurable battery charger. It is composed from two power stages. The first stage is a full-bridge AC-DC bidirectional converter, the second is a full bridge isolate DC-DC converter [29-30]. According to the above description, the structure of the proposed charger shown in Figure 1 is on-board and single-phase with plug-in electric vehicle. The performance of the charger is evaluated by its power-conversion efficiency and power quality (i.e., total harmonic distortion and power factor) [31]. Choosing the appropriate filter in a vehicle charger can affect the quality of the charger and reduce the weight of the charger. The LC filter ( $L_f, C_f$ ) is usually designed to have a resonant frequency that is lower than the lowest harmonic frequency. If the converter is controlled using a PWM technique that has a fixed switching frequency, the design is rather simple because we can just choose a resonant frequency that is much lower than the switching frequency [32-34]. If the converter is controlled using a hysteresis controller that has a variable frequency, the lowest harmonic frequency is difficult to be determined. There is a possibility that the lowest harmonic frequency is equal to the resonant frequency of the LC filter. If the resonant frequency is designed very low, however, the filter size will be very large. In order to minimize the losses in the filter, The parasitic resistances of the filter should be designed very low. However, a combination of large LC filter with low parasitic resistances may generate oscillation problem and very slow response [35, 36]. To overcome this challenges, in this paper a new scheme of EV charging control proposed by injection virtual resistor to controller circuit and improve charger performance is proposed. This control method, without changing the capacity of the LC filter, is designed only to reduce the input harmonic. Isolated transformer is used to insulate the dc part of the mains electricity. And by separating the AC-DC controller and the DC-DC controller, it is possible to control the charger more easily.

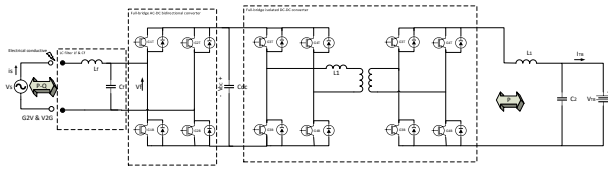


**Fig. 1. Reconfigurable battery charger composed by two power stages: full-bridge AC-DC bidirectional converter; full-bridge isolated bidirectional DC-DC converter [34, 35]**

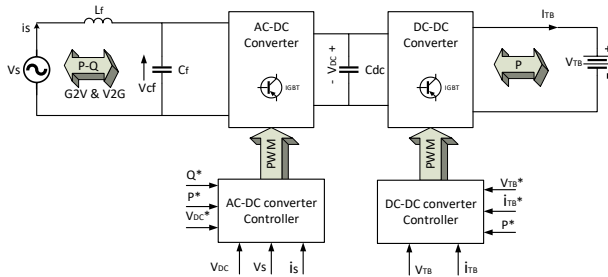


**Fig. 2. A view of the two control sections of the charger, the "\*" sign indicates the reference parameter [2, 34, 35]**

**2. CHARGER CONTROLLER STRUTURE**

The power flow in each converter depends on the operating mode. The G2V and V2G modes are shown in Figure 1. In G2V mode, the active power flows from the network to the DC-link and from the DC-link to the battery. In V2G mode, the active power passes in the opposite direction. In both modes of operation, the battery charger can keep the reactive power constant. The overview of the charger controller is shown in Figure 2, which includes two sections, the AC-DC converter controller and the DC-DC converter controller. The AC-DC converter controller is responsible for keeping the DC-link voltage (\$V\_{DC}\$) constant and controlling the active power \$P\$ and reactive power \$Q\$ of the charger according to the charge of the charger, which can be V2G or G2V. The DC-DC converter controller is responsible for controlling the battery power and is designed in two modes: constant current and constant voltage. Switching pulses of converter switches are created by pulse width modulation (PWM). This structure is used in light vehicles that use single-phase electricity for charging due to its ease of access. It is also estimated that in the future, electric vehicles will increase and the need to improve the performance of chargers from the vehicle to reduce THD fluctuations in the network. It would be appropriate to use this solution.

**2.1. DC-DC converter controller in G2V mode**

The DC link voltage of the charger is always higher than the battery voltage, so when working in G2V mode, the two-way DC-DC converter always acts as a buck converter. Most manufacturers of electric vehicle batteries recommend two charging step, constant current

until the maximum recommended voltage is reached and then in the second step, as long as the current consumed by the battery reaches a small amount, The voltage is kept constant. Figure 3 shows the charging steps for a single-cell Winston (90 Ah, 3.7 V) wbLYP90AHA battery.

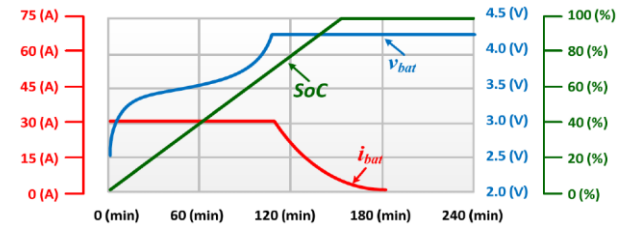


**Fig. 3. Two-step charging algorithm [34]**

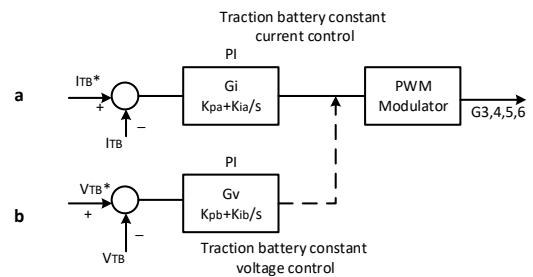


**Fig. 4. DC-DC converter controller in the G2V mode; a) constant current control, b) constant voltage control [34, 35]**

In order to implement the recommendations of car manufacturers, in G2V mode, the DC-DC converter according to Figure 4 is controlled as a buck converter by the PI controller as both a constant current and a constant voltage. In the controller DC-DC, the power factor value is determined using \$P^\*\$ and \$Q^\*\$.

In constant current step, the current reference is compared to the actual current, and the current error is given to the PI controller to set the (D) duty-cycle of the PWM modulator. When the battery voltage reaches the maximum recommended value by the manufacturers, the control algorithm changes to a constant voltage step. During these steps, the output voltage of the DC-DC converter is kept constant by the second PI controller. It is worth mentioning, that the DC-DC converter conversion function in battery charge mode is Equation 1. \$W\_2\$ is considered infinite in G2V mode with a suitable approximation.

$$H_1 = \frac{G_{d0} \left(1 - \frac{s}{w_2}\right)}{1 + \frac{s}{Qw_0} + \left(\frac{s}{w_0}\right)^2} = \frac{\frac{V_{dc}}{D}}{1 + \frac{s}{R} + LCs^2} \tag{1}$$

$$G_{d0} = V_{dc}/D; w_2 = \infty; w_0 = \frac{1}{\sqrt{LC}}; Q = R\sqrt{C/L}$$

**2.2. DC-DC converter controller in V2G mode**

In order to give the AC-DC bidirectional converter the ability of delivering the energy stored in the battery to the network. The DC link voltage \$V\_{dc}\$, must be higher

than the network voltage peak. So, the DC-DC converter has to work as a boost converter. Knowing that the battery voltage is not affected by fluctuations during small time periods, it is possible to adjust the reactive power supplied to the network by applying the constant current. When the battery voltage decreases during the charging process, in order to keep the active power constant, it is necessary to increase the current reference received from the battery, reference i.e.  $i_{TB}^*$ . The resulting battery current is compared to the actual current as the reference current and the error obtained according to Figure 5 is given to the PI controller and the ( $D'$ ) duty-cycle controls the PWM modulator. It should be noted that the conversion function of DC-DC converter in battery discharge mode is given in the Equation 2.

$$H_1 = \frac{G_{d0} \left(1 - \frac{s}{w_2}\right)}{1 + \frac{s}{Qw_0} + \left(\frac{s}{w_0}\right)^2} = \frac{\frac{V_{dc}}{D'} \left(1 - \frac{L}{RD'^2 s}\right)}{1 + \frac{L}{RD'} s + LCs^2} \quad (2)$$

$$G_{d0} = V_{dc}/D'; w_2 = \frac{D'^2 R}{L}; w_0 = \frac{1}{\sqrt{LC}}; Q = D'R\sqrt{C/L}$$

### 2.3. AC-DC converter controller G2V

In order to comply with maximum independent current harmonics specified by the IEC 61000-3-2 standard, the full bridge AC-DC bidirectional converter needs to be fully synchronized with the main voltage. Therefore, the phase-locked loop (PLL) algorithm needs to be run as the first algorithm by the controller. Figure 6 shows the single-phase PLL diagram block. The feedback signals  $PLL\alpha$  and  $PLL\beta$  in the PLL algorithm are generated by  $\sin(\omega t)$  and  $\cos(\omega t)$ , respectively ( $\omega$  is the frequency angle of the power grid). These signals have a unit size that is multiply by  $\sqrt{2}$ , and the  $PLL\alpha$  is ninety degrees ahead of the  $PLL\beta$ . When the PLL is synchronize,  $PLL\alpha$  and  $PLL\beta$  signals are direct and square components (with a phase difference of 90) of the main voltage. These signals are sent as input to subsequent control algorithms.

The reference current of the  $i_{in}^*$  AC-DC bidirectional converter is obtained by adding two components. One is related to active power and the order is related to reactive power. The active power of  $P^*$  is directly related to the battery charging current and is regulated by the PI controller to regulate the voltage of the DC link. The second component is  $Q^*$  reactive power, that transformer produced or absorbed, and is defined as the external input parameter. Both active and reactive powers are affected by the direct component  $PLL\alpha$  and the square component  $PLL\beta$ . Figure 7 shows the diagram block of the full bridge AC-DC bidirectional converter controller to generate  $i_{in}^*$  reference current

which uses pulse width modulation (PWM) control method to control AC-DC converter.

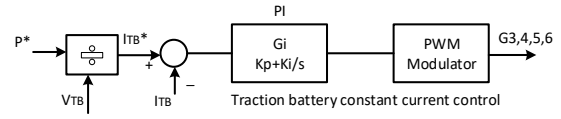


Fig. 5. DC-DC converter controller in the V2G mode [34, 35]

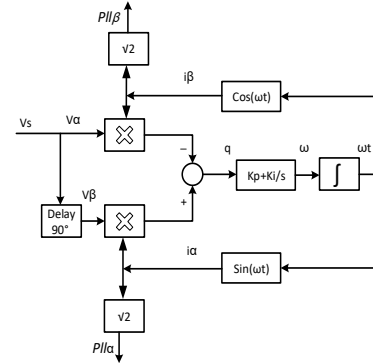


Fig. 6. PLL [34, 35]

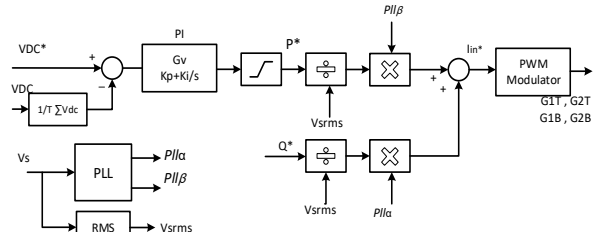


Fig. 7. AC-DC converter controller [34, 35]

It should be noted that the maximum amount of reactive power that the converter can produce is limited by the apparent power of the bidirectional AC-DC converter. Due to the sinusoidal current on the AC side, the available reactive is in from of Equation 3 [34, 35]:

$$Q = \sqrt{S^2 - P^2} \quad (3)$$

The above relationship means that the reactive power available depends on the active power given to the battery. The power given to the battery during the charging process changes. Considering that during the cycle, the battery is charged at a constant power, And that means it is not attracted the constant power from AC side. the constant power from the AC side, there needs to be a central energy source in the system. For this purpose, the battery charger uses the DC link capacitor. Because the energy stored in the capacitor changes during charging, voltage swings with the frequency of  $2\omega$ . In order to avoid damping these fluctuations on current reference, the average voltage of DC link is given to the controller. Therefore, the PI controller only controls the average voltage of the DC link in the capacitor. And it allows the battery to be charged at a constant power and receive a constant-sized sinusoidal current from the power grid.

**2.4. AC-DC converter controller in V2G mode**

In order to make the AC-DC converter work as an inverter, the full bridge AC-DC bidirectional converter must be synchronized with the main voltage. The synchronization operation is performed using the PLL algorithm described in the previous sections. As with the G2V, in the V2G mode the  $i_{in}^*$  full bridge AC-DC converter is a whole set of two components, one for active power and one for reactive power. These powers are defined as external input parameters. With this in mind, the control algorithm implemented in V2G mode is similar to G2V mode.

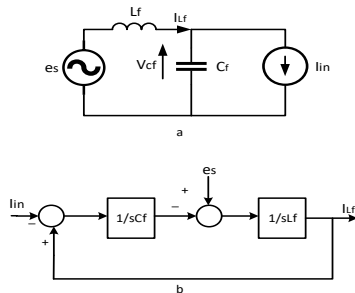


**Fig. 8. a) Charger equivalent circuit. b) Charger block diagram [36-41]**

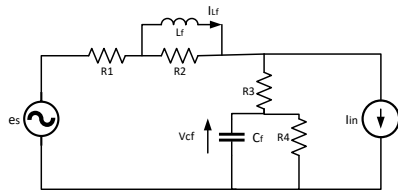


**Fig. 9. Four possible resistance connections in an LC filter [36-41]**

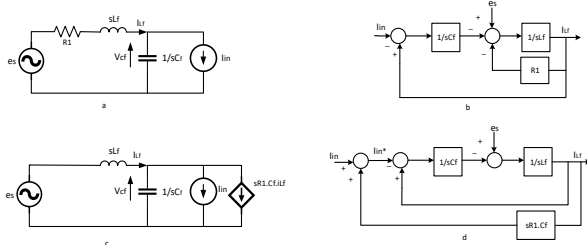


**Fig. 10. a) Charger equivalent circuit with real resistor  $R_1$  series with inductor. b) Charger diagram block with real resistor  $R_1$  series with inductor. c) Charger equivalent circuit with injection of virtual resistor by depended source. d) Charger diagram block with injection of virtual resistor by inductor current feedback**

**3. THE CONCEPT OF VIRTUAL RESISTANCE**

High oscillations in the LC circuit can be attenuated by a resistor connected to the LC circuit. Although damping oscillations are very effective using resistors, they cannot be used at high power due to high losses. Understanding the basic principles of damping oscillation in an LC circuit using a resistor is suggested as the basis of the concept of virtual resistance. Figure 8a shows a single-phase AC equivalent circuit in an AC-DC PWM converter. The  $i_{in}$  current source is an essential component of the AC-DC phase input of the

PWM converter, which is assumed to be the reference input current used to control the converter.  $e_s$  is the phase source voltage. Figure 8b shows a block diagram that can be used to analyze the dynamic behavior of a circuit in figure 8a. Based on the block diagram in figure 8b, the equations 4 and 5 can be obtained:

$$\frac{I_s}{I_{in}} = \frac{1}{1+s^2L_fC_f} \tag{4}$$

$$\frac{V_{cf}}{I_{in}} = \frac{-sL_f}{1+s^2L_fC_f} \tag{5}$$

$I_s(s)$  is the source current,  $V_{cf}(s)$  is the filter capacitor voltage,  $I_{in}(S)$  is the input current.  $S$  is the Laplace operator. Equations (4) and (5) show that the adverse transient in the source current and capacitive voltage is generated when the input current of the converter suddenly changes. In practice, oscillations in the LC circuit are usually damped by losses. This can be done using a resistor connected to an LC filter. The resistor can be connected in series or in parallel to the inductor or filter capacitor. Figure 9 shows four possible resistance connections in an LC filter.

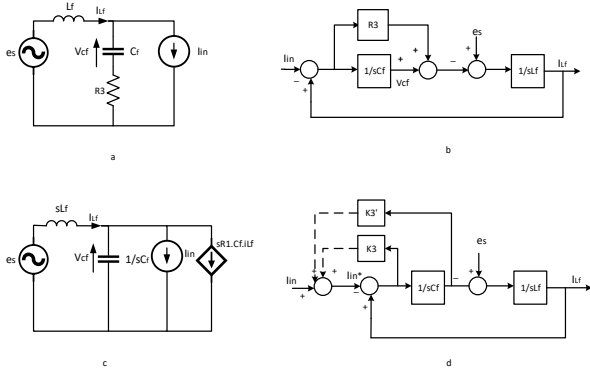
Using a real resistor to damp the oscillation significantly reduces system performance. So, it can be replaced with a virtual resistor with no losses, resulting in oscillation deletion without reducing efficiency.

**3.1. Virtual resistance series with inductor**

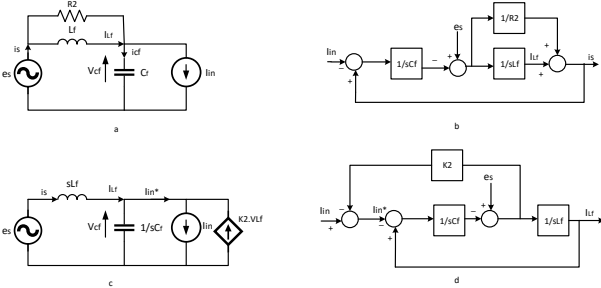
In Figure 10 a single-phase rectifier equivalent circuit is shown, the  $R_1$  resistor is located in series with filter inductance. The equivalent block diagram is shown in Figure 10b. With a little manipulation, the Figure circuit 10b can be converted to circuit in Figure 10d. In both circuits, the role of the  $R_1$  series resistor, which is proportional to the inductance current, behaves similarly. In Figure 10d, virtual resistance is used instead of real resistance. The derivative of the inductance current is multiplied by the constant value of  $C_fR_1$ . The output ( $i_{Lf} s C_fR_1$ ) is injected into the  $i_{in}$  current and collected. In Figure 10c, there is no real resistance and its role is played by the dependent current source.

Figure 10b is used to analyze the circuit dynamics from which the transfer function 6 is obtained. Compared to equation 4, the term  $sR_1C_f$  has been added to the denominator of the conversion function, which is effective in the stability of the conversion function and shows the effect of resistance  $R_1$  on the circuit. This effect can be seen from Nyquist diagram which is stated in the following sections.

$$\frac{I_s}{I_{in}} = \frac{1}{1+sR_1C_f+s^2L_fC_f} \tag{6}$$



**Fig. 11. a) Charger equivalent circuit with real resistor  $R_3$  series with capacitor. b) Charger diagram block with real resistor  $R_3$  series with capacitor. c) Charger equivalent circuit with injection of virtual resistor by depended source. d) Charger diagram block with injection of virtual resistor by capacitor current feedback [36-38]**



**Fig. 12. a) Charger equivalent circuit with real resistor  $R_2$  parallel with inductor. b) Charger diagram block with real resistor  $R_2$  parallel with inductor. c) Charger equivalent circuit with injection of virtual resistor by depended source. d) Charger diagram block with injection of virtual resistor by inductor voltage feedback**

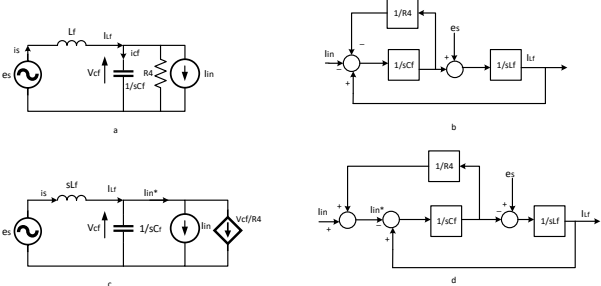


**Fig. 13. a) Charger equivalent circuit with real resistor  $R_4$  parallel with capacitor. b) Charger diagram block with real resistor  $R_4$  parallel with capacitor. c) Charger equivalent circuit with injection of virtual resistor by depended source. d) Charger diagram block with injection of virtual resistor by capacitor voltage feedback [36-38]**

**3.2. Virtual resistor series with capacitor**

With a similar process, Virtual resistance equal resistance  $R_3$  can be created. Figure 11a shows the single-phase equivalent charger circuit and Figure 11b shows its equivalent diagram block.

The figure 11b shows the diagram block conversion function of Equation 7. Compared to Equation 4, the  $sR_3C_f$  parameter is added to the denominator and the divider. Figure 11c shows the circuit equivalent to a single-phase charger by injecting virtual resistance

through a dependent source. In the 11d diagram block, by applying the feedback  $K_3 = -sR_3C_f / (1 + sR_3C_f)$  from  $i_{cf}$  i.e. capacitor current, a similar behavior can be created with the capacitor series resistance. By changing the virtual resistance of  $R_3$ , the dynamic behavior of the charger can be positively affected.

$$\frac{I_s}{I_{in}} = \frac{1 + sR_3C_f}{1 + sR_3C_f + s^2L_fC_f} \tag{7}$$

However, to get rid of the derivative in  $K_3$ , feedback can be injected from the capacitor voltage  $V_{cf}$  and the coefficient  $K_3 = R_3 \cdot (-C_f/L_f)$  can be used and the Equation 8 can be obtained.

$$\frac{I_s}{I_{in}} = \frac{1}{1 + sR_3C_f + s^2L_fC_f} \tag{8}$$

Equation 7 is drawn in green and Equation 8 is drawn in blue. Both equations 7 and 8 behave similarly. The main reason for using Equation 8 is to remove the derivative from Equation 7 for ease of implementation of the controller As shown in Figures 10 and 11, implementing a series of virtual resistors with an inductor or filter capacitor requires an additional and derivative current sensor. The derivative may cause noise problems because it amplifies high-frequency signals. Applying a parallel resistor to the inductor and filter capacitor can also be effective in reducing oscillations.

**3.3. Virtual resistance parallel to inductance**

Figure 12 shows the equivalent circuit and diagram block applying  $R_2$  resistors parallel to the filter inductor. The conversion function of the 12b diagram block flow is shown in Equation 9, where the expression  $sL_f/R_2$  is added in comparison with Equation 4 in the denominator and the divided. Which affects the damping oscillations of the charger input current. By applying the feedback  $K_2 = (-S_2 \cdot L_f \cdot C_f) / (R_2 + S \cdot L_f)$  to Equation 9. However, the implementation of such a control block due to the presence of S-derivative creates noise problems and increases the range of disturbances.

$$\frac{I_s}{I_{in}} = \frac{1 + sL_f/R_2}{1 + sL_f/R_2 + s^2L_fC_f} \tag{9}$$

Therefore, by applying feedback  $K_2 = 1/R_2$  in Figure 12c, Equation 10 is obtained and a behavior similar to the parallel resistance with the inductor in the control block is seen. Both equations 9 and 10 behave similarly. The main reason for using Equation 10 is to remove the derivative from Equation 9 for ease of controller implementation.

$$\frac{I_s}{I_{in}} = \frac{1}{1 + sL_f/R_2 + s^2L_fC_f} \tag{10}$$

**3.4. Virtual resistance parallel to capacitor**

The  $R_4$  resistor has a similar function in reducing oscillations of the charger input current by connecting

the filter capacitor in parallel. The equivalent circuit is shown in Figure 13a. The application of virtual resistance  $R_4$  can be seen in the 13d diagram block conversion function shown in Equation 11.

$$\frac{I_s}{I_{in}} = \frac{1}{1 + sL_f/R_4 + s^2L_fC_f} \quad (11)$$

The addition of the  $sL_f/R_f$  parameter in Equation 11 denominator indicates the effect of virtual resistance on the charger.

#### 4. CHECK THE PERFORMANCE OF THE SYSTEM FOR THE SYSTEM FOR THE APPLICATION OF VIRTUAL RESISTANCE USING THE BODE AND NYQUIST DIAGRAMS

Based on the relationships obtained in the previous section, the Bode and Nyquist diagrams can be plotted and the system performance can be observed for the application of virtual resistance. For example, we consider the equivalent circuit of Figure 13, in which the resistor  $R_4$  is used in parallel with the filter capacitor. In Figure 14, the Bode and Nyquist diagrams plotted by changing the resistance  $R_4$  in Equation 11. Reducing the resistance  $R_4$  indicates an increase in system stability. This comparison can be seen similarly to other resistors. In the Figure 14, the parameters " $(R_{4red} < R_{4blue} < R_{4green})$ " are used to separate the red, blue and green colors of the diagram.

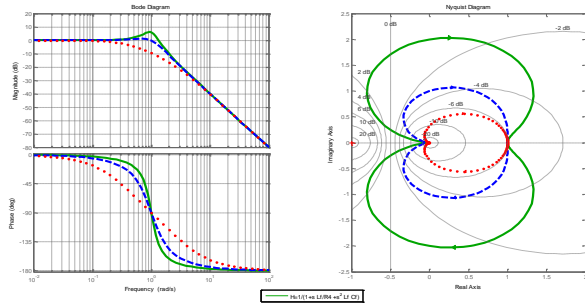


Fig. 14. The Bode and Nyquist diagram plotted by changing the resistance  $R_4$  According to Equation 11 ( $R_{4red} < R_{4blue} < R_{4green}$ )

#### 5. THE PROPOSED METHOD

In the previous sections, the structure of the AC-DC controller and the method of applying virtual resistance have been described. In this section, the intention is to improve the performance of the AC-DC controller by applying virtual resistance feedback to the AC-DC controller. Among the virtual resistances expressed, the  $R_4$  resistance feedback is shown in the Nyquist and Bode diagrams. In the virtual resistor parallel to capacitor  $R_4$ , a voltage sensor is used on the capacitor voltage and also in the feedback which does not need a derivative and these two features facilitate its

implementation. Due to the virtual resistance feedback in Figure 13d, to apply virtual resistance to the AC-DC controller in Figure 7, feedback from the capacitor voltage of the  $V_{cf}$  filter is required. The coefficient of  $1/R_4$  determines the amount of virtual resistance in feedback. Figure 15 shows the proposed control diagram block for applying virtual resistances.

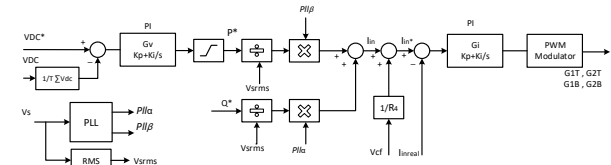


Fig. 15. The proposed method by apply virtual resistance in AC-DC converter control to reduce charger input current harmonics

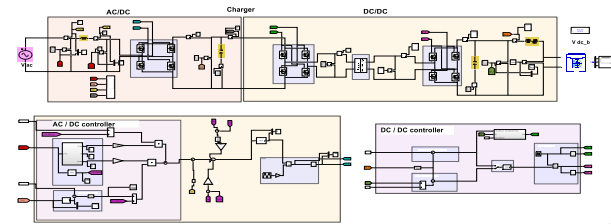


Fig. 16. An overview of the simulation of the MATLAB environment

#### 6. SIMULATION RESULTS

According to the controller introduced by injecting virtual resistance in Figure 15, for G2V and V2G performance modes in steady state, the charger circuit is simulated in MATLAB software. An overview of the simulation of the MATLAB environment is shown in figure 16. The purpose of this paper is to reduce the THD of the charger input current, in the steady state. And the study of transient states due to sudden load changes and network fluctuations, can be included in future research. In the text, the review is expressed in a steady state. For implementation, the ARM processor is suitable for this purpose due to its high switching frequency and good performance in the vehicle audio environment.

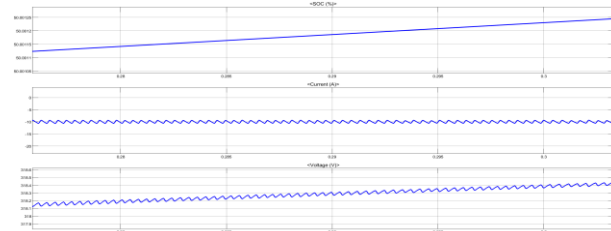


Fig. 17. SOC changes, current and voltage of battery in the G2V mode with virtual resistor injection

The results are compared with the control method without virtual resistance in Figure 7. In G2V performance mode, the charger receives power from the power network. The reference current for the battery charger is 10 amps. It should be noted that the value of

reactive power is zero. The initial battery charger rate is 50%. Voltage changes, battery current and SOC charging mode in G2V mode are shown in Figure 17.

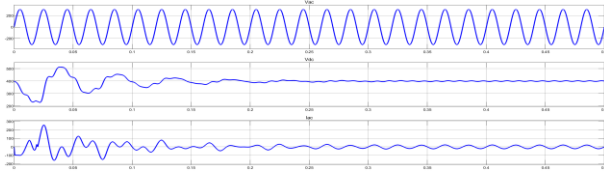


Fig. 18. the voltage and current of the network input ( $V_{ac}$ ,  $I_{ac}$ ) and the voltage of the DC-link ( $V_{dc}$ ) in G2V mode with virtual resistor injection

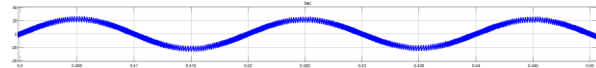


Fig. 19. Charger input current without virtual resistance (THD=4.5%)

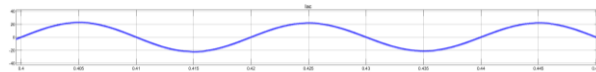


Fig. 20. charger input current with virtual resistance (THD=3.67%)

In Figure 18, the charger input voltage and current i.e.  $V_{ac}$  and  $I_{ac}$  and also the DC-link charger voltage is shown. As the charger voltage and current have the same phase angle. It can be deduced that the charger works with unity power factor.

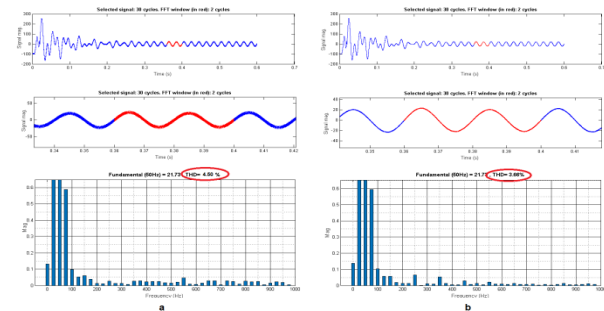


Fig. 21. Charger input current and harmonic diagram of charger input current. a) Without virtual resistance. b) With virtual resistance

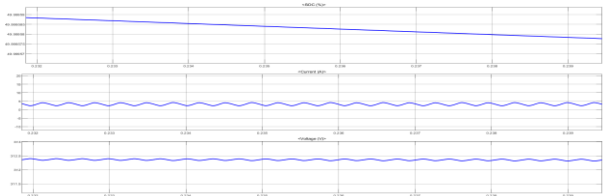


Fig. 22. SOC changes, current and voltage of battery in the V2G mode with virtual resistor injection

Simulation with a controller without virtual resistance is also performed. The THD of the charger input current is 4.5 percent, which is in accordance with the standard and less than 5 percent. The results obtained in the simulation of the controller with virtual resistance in G2V mode indicate that the THD current received from the network is low, equal to 3.67% which is 0.81 percent less than before. By injecting virtual resistance, the harmonic value of the input current ( $i_{ac}$ ) from the

network is reduced and the charger performance is improved. Figs. 19-21 show the input current diagram to the charger and THD input mode in two modes without and with virtual resistance.

In V2G mode, the charger gives power to the network. The full bridge AC-DC converter controller is similar to the G2V mode, and the DC-DC converter controller is in V2G mode. The active power of the reference in V2G mode is 1 kw. It should be noted that the amount of reactive power in the simulation is zero. As seen in Figure 22, the battery charge is reduced. Also, in the V2G mode with virtual resistance injection reduces input current THD in the charger. Harmonic reduction of the input current reduces the distortion power and consequently increases the efficiency.

### 7. CONCLUSIONS

The presence of current harmonics distortion caused by electric vehicle chargers exacerbates the oscillations of the power grid and impacts its stability. As an attempt toward solving this issue with minimum hardware alteration, this article examined the configuration of an on-board charger with a single-phase electrical connection, due to its versatility in light passenger cars, then proposed injection of a virtual resistant for improving the controller performance. The use of the idea of injecting virtual resistance in the AC-DC converter controller in steady state indicated the proper performance of the charger in reducing input current THD. In addition, the DC voltage ripple of batteries was reduced in order to increase the battery life. Sudden load changes as well as transient fluctuations in the power grid can damage the charger electronics equipment of the charger. Further research could be done to reduce fluctuations in transient states using the idea of virtual resistance injection.

### REFERENCES

- [1] S. Haghbin, S. Lundmark, M. Alakula and O. Carlson, "Grid-connected integrated battery chargers in vehicle applications: Review and new solution", *IEEE Trans. Ind. Electron.*, vol. 60, pp. 459-73, 2012.
- [2] M. Yilmaz and P.T. Krein, "Review of battery charger topologies, charging power levels, and infrastructure for plug-in electric and hybrid vehicles", *IEEE Trans. Power Electron.*, vol. 28, pp. 2151-69, 2012.
- [3] A. Khaligh and S. Dusmez, "Comprehensive topological analysis of conductive and inductive charging solutions for plug-in electric vehicles", *IEEE Trans. Veh. Technol.*, vol. 61, pp. 2475-89, 2012.
- [4] S. Jeong et al., "Electrolytic capacitor-less single-power-conversion on-board charger with high efficiency", *IEEE Trans. Ind. Electron.*, vol. 63, pp. 7488-97, 2016.
- [5] B. Whitaker et al., "A high-density, high-efficiency, isolated on-board vehicle battery charger utilizing silicon

- carbide power devices”, *IEEE Trans. Power Electron.*, vol. 29, pp. 2606-17, 2013.
- [6] D. Gautam et al., “An automotive onboard 3.3-kW battery charger for PHEV application”, *IEEE Trans. Veh. Technol.*, vol. 61, pp. 3466-74, 2012.
- [7] S. Kim and F. Kang, “Multifunctional onboard battery charger for plug-in electric vehicles”, *IEEE Trans. Ind. Electron.*, vol. 62, pp. 3460-72, 2014.
- [8] K. Yao, Y. Wang, J. Guo and K. Chen, “Critical conduction mode boost PFC converter with fixed switching frequency control”, *IEEE Trans. Power Electron.*, vol. 33, pp. 6845-57, 2017.
- [9] T. Mishima, K. Akamatsu and M. Nakaoka, “A high frequency-link secondary-side phase-shifted full-range soft-switching PWM DC–DC converter with ZCS active rectifier for EV battery chargers”, *IEEE Trans. Power Electron.*, vol. 28, pp. 5758-73, 2013.
- [10] M. Kwon and S. Choi, “An electrolytic capacitorless bidirectional EV charger for V2G and V2H application”, *IEEE Trans. Power Electron.*, vol. 32, pp. 6792-9, 2016.
- [11] K. Yoo, K. Kim and J. Lee, “Single-and three-phase PHEV onboard battery charger using small link capacitor”, *IEEE Trans. Ind. Electron.*, vol. 60, pp. 3136-44, 2012.
- [12] L. Wang, B. Zhang and D. Qiu, “A novel valley-fill single-stage boost-forward converter with optimized performance in universal-line range for dimmable LED lighting”, *IEEE Trans. Ind. Electron.*, vol. 64, pp. 2770-8, 2016.
- [13] Y. Wang et al., “A single-stage LED driver based on SEPIC and LLC circuits”, *IEEE Trans. Ind. Electron.*, vol. 64, pp. 5766-76, 2016.
- [14] G. Moschopoulos and P. Jain, “Single-phase single-stage power-factor-corrected converter topologies”, *IEEE Trans. Ind. Electron.*, vol. 52, pp. 23-35, 2005.
- [15] S. Li, J. Deng and C. Mi, “Single-stage resonant battery charger with inherent power factor correction for electric vehicles”, *IEEE Trans. Veh. Technol.*, vol. 62, pp. 4336-44, 2013.
- [16] J. Lee, Y. Yoon and J. Kang, “A single-phase battery charger design for LEV based on DC-SRC with resonant valley-fill circuit”, *IEEE Trans. Ind. Electron.*, vol. 62, pp. 2195-205, 2014.
- [17] N. Trong et al., “Modified current-fed full-bridge isolated power factor correction converter with low-voltage stress”, *IET Power Electron.*, vol. 7, pp. 861-7, 2013.
- [18] C. Li, Y. Zhang, Z. Cao and X. Dewei, “Single-phase single-stage isolated ZCS current-fed full-bridge converter for high-power AC/DC applications”, *IEEE Trans. Power Electron.*, vol. 32, pp. 6800-12, 2016.
- [19] S. Lee and H. Do, “Single-stage bridgeless AC–DC PFC converter using a lossless passive snubber and valley switching”, *IEEE Trans. Ind. Electron.*, vol. 63, pp. 6055-63, 2016.
- [20] W. Choi, “Single-stage battery charger without full-bridge diode rectifier for light electric vehicles”, *Electron. Lett.*, vol. 47, pp. 617-8, 2011.
- [21] W. Choi and J. Yoo, “A bridgeless single-stage half-bridge AC/DC converter”, *IEEE Trans. Power Electron.*, vol. 26, pp. 3884-95, 2011.
- [22] D. Gautam et al., “An automotive onboard 3.3-kW battery charger for PHEV application”, *IEEE Trans. Veh. Technol.*, vol. 61, pp. 3466-74, 2012.
- [23] P. Sinusoidal, “Non sinusoidal, balanced or unbalanced conditions”, *IEEE Std.*, pp. 1459-2000, 2009.
- [24] K. Kim et al., “Battery charging system for PHEV and EV using single phase AC/DC PWM buck converter”, *IEEE Veh. Power Propul. Conf.*, 2010.
- [25] M. Pahlevaninezhad et al., “A new control approach based on the differential flatness theory for an AC/DC converter used in electric vehicles”, *IEEE Trans. Power Electron.*, vol. 27, pp. 2085-103, 2011.
- [26] L. Huber, Y. Jang and M. Jovanovic, “Performance evaluation of bridgeless PFC boost rectifiers”, *IEEE Trans. Power Electron.*, vol. 23, pp. 1381-90, 2008.
- [27] R. Metidji, B. Metidji and B. Mendil, “Design and implementation of a unity power factor fuzzy battery charger using an ultrasparse matrix rectifier”, *IEEE Trans. Power Electron.*, vol. 28, pp. 2269-76, 2012.
- [28] X. Zhou et al., “Multi-function bi-directional battery charger for plug-in hybrid electric vehicle application”, *IEEE Energy Convers. Congr. Exposition*, 2009.
- [29] D. Erb, O. Onar and A. Khaligh, “Bi-directional charging topologies for plug-in hybrid electric vehicles. In 2010 Twenty-Fifth Annual”, *IEEE Appl. Power Electron. Conf. Exposition*, 2010.
- [30] V. Monteiro et al., “Batteries charging systems for electric and plug-in hybrid electric vehicles”. *New Adv. Veh. Technol. Autom. Eng.*, 2012.
- [31] O. Onar, J. Kobayashi, D. Erb and A. Khaligh, “A bidirectional high-power-quality grid interface with a novel bidirectional noninverted buck–boost converter for PHEVs”, *IEEE Trans. Veh. Technol.*, vol. 61, pp. 2018-32, 2012.
- [32] Y. Lee, A. Khaligh and A. Emadi, “Advanced integrated bidirectional AC/DC and DC/DC converter for plug-in hybrid electric vehicles”, *IEEE Trans. Veh. Technol.*, vol. 58, pp. 3970-80, 2009.
- [33] S. Kim, H. Song and K. Nam, “Idling port isolation control of three-port bidirectional converter for EVs”, *IEEE Trans. Power Electron.*, vol. 27, pp. 2495-506, 2011.
- [34] J. Pinto, V. Monteiro, H. Gonçalves and J. Afonso, “Onboard reconfigurable battery charger for electric vehicles with traction-to-auxiliary mode”, *IEEE Trans. Veh. Technol.*, vol. 63, pp. 1104-16, 2013.
- [35] G. Choe et al., “A Bi-directional battery charger for electric vehicles using photovoltaic PCS systems”, *IEEE Veh. Power Propul. Conf.*, 2010.
- [36] P. Dahono, “A control method to damp oscillation in the input LC filter”, *IEEE 33rd Annu. Power Electron. Specialists Conf.*, 2002.
- [37] P. Dahono, Y. Bahar, Y. Sato and T. Kataoka, “Damping of transient oscillations on the output LC filter of PWM inverters by using a virtual resistor”, *4th IEEE Int. Conf. Power Electron. Drive Syst.*, 2001.
- [38] A. Adapa and V. John, “Virtual resistor based active damping of LC filter in standalone voltage source inverter”, *IEEE Appl. Power Electron. Conf. Exposition*, 2018.
- [39] U. Erburu et al., “Parameter-independent control for battery chargers based on virtual impedance emulation”, *IEEE Trans. Power Electron.*, vol. 33, pp. 8848-58, 2018.
- [40] Y. Fu et al., “Imbalanced load regulation based on virtual resistance of a three-phase four-wire inverter for EV vehicle-to-home applications”, *IEEE Trans. Transp. Electrification*, vol. 5, pp. 162-73, 2018.
- [41] A. Urtasun et al., “Parameter-independent battery control based on series and parallel impedance emulation”, *IEEE Access*, vol. 7, pp. 70021-31, 2019.